Modelling of cross-flow membrane contactors

Dindore, V. Y.; Brilman, D. W. F.; Versteeg, G. F.

Published in:
Journal of Membrane Science

DOI:
10.1016/j.memsci.2004.11.017

Publication date:
2005

Available online at www.sciencedirect.com
SCIENCE DIRECT®
Journal of Membrane Science 251 (2005) 209–222
journal of MEMBRANE SCIENCE
www.elsevier.com/locate/memsci

Modelling of cross-flow membrane contactors: physical mass transfer processes

V.Y. Dindore[a,*], D.W.F. Brilman[c], G.F. Versteeg[b]

[a] *NTNU, Institute for Kjemisk Processteknologi, K-5, N-7491, Trondheim, Norway*
[b] *Design and Development of Industrial Processes, Faculty of Chemical Technology, University of Twente, P.O. Box 217, 7500AE Enschede, The Netherlands*
[c] *Sasol Technology Netherlands B.V., Hallenweg 5, 7522 NB Enschede, The Netherlands*

Received 14 May 2004; accepted 2 November 2004
Available online 19 January 2005

Abstract

Traditionally, hollow fiber membrane contactors used for gas–liquid contacting were designed in a shell and tube configuration with shell-side fluid flowing parallel to the fiber-side fluid, either in co-current or counter-current pattern. The primary limitations of these so-called 'parallel flow' contactors are the shell-side flow channeling or mal-distribution due to non-uniform packing of the hollow fibers, higher shell-side pressure drop and relatively lower mass transfer coefficients. These limitations can be eliminated or reduced substantially by placing hollow fibers perpendicular to the flow direction. In these cross-flow membrane contactors the concentrations of both fluids vary in both directions i.e. in the direction of the flow as well as in the direction perpendicular to the flow. Hence, unlike parallel flow contactors, simple logarithmic averaging of the concentration driving force cannot be used to predict performance of the cross-flow membrane contactors. Similar changes in the driving force are also found in the cross-flow shell and tube heat exchanger. An analytical expression based on heat transfer analogy is derived in this work to describe the mass transfer in these hollow fiber cross-flow contactors. However, it was found that when the change in the volumetric flow of the compressible fluid is significant heat transfer analogy cannot be used to predict the performance of the cross-flow gas–liquid membrane contactor. Therefore, a detailed numerical model is developed to analyze the performance of the cross-flow membrane contactor in such cases. The model takes into account the shell-side mixing, change in concentration driving force in all direction as well as cascading two or more cross-flow modules to give overall co- or counter-current flow arrangement. To validate the model and developed analytical expression, carbon dioxide absorption experiments were carried out in cross-flow membrane contactor using water as a solvent. The predictions of the developed numerical model were found to be in good agreement with the experimental results.

Keywords: Hollow fiber membranes; Membrane contactors; CO_2 absorption; Cross-flow; Modelling

1. Introduction

The use of micro-porous membranes for indirect contacting of two immiscible phases, such as gas and liquid, without dispersing one phase into another is a relatively new concept. The relative merits of these membrane contactors are operational flexibility, high mass transfer rates, compactness and easy scale up [4]. These unparalleled advantages over the conventional column type of contactor seem to make the membrane contactors ideal for various industrial gas–liquid contacting processes. In general hollow fiber membrane contactors are preferred over flat sheet membrane contactors due to the higher interfacial area. Based on the flow directions of the gas and liquid phase, the hollow fiber membrane contactor can be used in two different modes of operation.

1. *Parallel flow mode*: the flow of the both phases is parallel to the axis of the fiber and both fluids flow either in same direction (co-current) or in opposite direction (counter-current).

* Corresponding author. Tel.: +47 73594598; fax: +47 73594080.
E-mail address: vishwas.dindore@chemeng.ntnu.no (V.Y. Dindore).

0376-7388/$ – see front matter © 2004 Elsevier B.V. All rights reserved.
doi:10.1016/j.memsci.2004.11.017

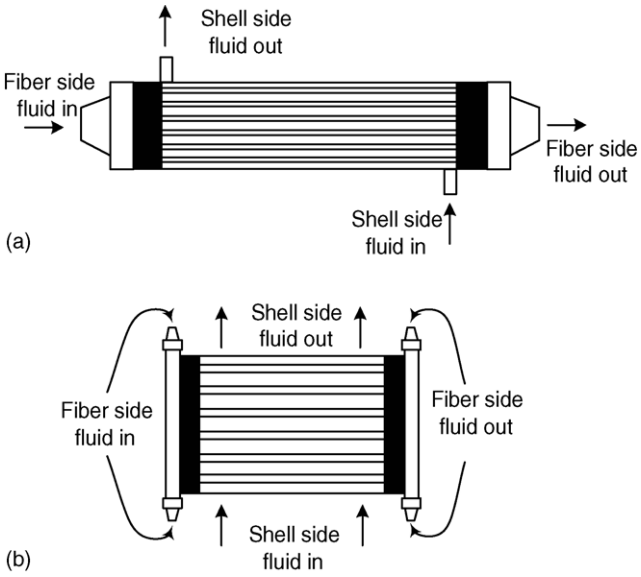

Fig. 1. (a) Parallel-flow hollow fiber module; (b) cross-flow hollow fiber module.

2. *Cross-flow mode*: the shell-side fluid flows perpendicular to the axis of fiber. Thus the two fluids flow at right angles to each other.

The operation principle of these modes of operation is shown in Fig. 1a and b. Parallel flow offers the highest average concentration driving force in the case of counter-current flow and is preferred in situations where membrane or fiber-side mass transfer resistance controls [13]. However, when the shell-side mass transfer resistance is significant, cross-flow operation is preferred as it offers several advantages such as relatively high mass transfer coefficients, minimized shell-side channeling and lower shell-side pressure drop when compared to the parallel flow contactors [14]. Jansen et al. [7] used the cross-flow membrane module for the reactive absorption of SO_2 and found that mass transfer coefficient for the cross-flow modules are typically one order of magnitude higher than that for the conventional parallel flow modules. In addition, these authors also found that the shell-side pressure drop was considerably lower than that for the conventional parallel flow modules. This difference in the module performance is mainly due to the flow path taken by the shell-side fluid. The differences in shell-side fluid paths affect module performance in two ways. First, the extent of mass transfer varies from streamline to streamline due to the residence time distribution and channeling of the shell-side fluid. The spread in residence time and shell-side channeling result in lower mass transfer rates. Moreover, severe mal-distribution of shell-side fluid may also result in dead zone formations. As cross-flow operation has reduced shell-side channeling and lesser possibility of shell-side fluid mal-distribution as compared to the parallel flow contactors, the performance of the cross-flow contactor is better. Secondly, the local mass transfer coefficient is a function of local velocity and turbulence. In case of cross-flow contactors the concentration boundary layer break-up occurs due to continuous splitting and remixing of the shell-side fluid resulting into more turbulence in the mass transfer zone. Hence the mass transfer coefficient obtained in the cross-flow contactors turns out to be higher as compared to the parallel flow contactors. In industry, these rectangular cross-flow modules are commercialized by TNO Environmental Energy and Process Innovation [5] and by Kvaerner Oil & Gas in co-operation with W.L. Gore & Associates GmbH [6] for CO_2 capture from various gas streams. Furthermore, other commercial applications such as removal of NO_x and SO_2 from waste-incineration off-gas, removal of mercury, H_2S and water from natural gas, removal of VOC from gas streams, etc. can be envisaged.

The mode of operation of membrane contactor can significantly affect the design and construction of the module. In case of the cross-flow membrane contactors the concentrations of both fluids vary in both directions i.e. in the direction of the flow and in the direction perpendicular to the flow. Hence, unlike parallel flow contactors, simple logarithmic averaging of the concentration driving force cannot be used to predict the performance of the cross-flow contactors. This makes the design of cross-flow membrane contactor comparatively difficult. Similar local variations in the driving force with position are also found in the cross-flow heat exchanger. However, in the case of cross-flow membrane gas–liquid contactors along with the change in the concentrations the volumetric flow of the gas phase can also change significantly over the volume of the module. Therefore the performance of these types of contactors needs to be analyzed by detailed mathematical modelling.

Wang and Cussler [13] modeled a baffled rectangular cross-flow membrane contactor using iterative and finite difference methods. However, in both methods authors used an averaged driving force and did not consider the change in driving force in all directions, nor the mixing on the shell side. Bergero and Chiari [2] studied and modeled the humidification/dehumidification process in a cross-flow membrane contactor. The steady state model developed by these authors assumes both phases to be completely mixed and uses bulk mean temperature and water concentration for water flux calculation. Furthermore in both of these works, the mass transfer coefficient on shell side as well as on fiber side was included as external input parameter.

In the present work, a numerical model is developed to describe and predict the performance of cross-flow membrane contactors. The model is based on first principles and takes into account shell-side mixing, change in concentration driving force in all directions as well as the cascading of two or more cross-flow modules to give overall co- or counter-current flow pattern. In addition, analytical expression analogous to heat transfer in cross-flow shell and tube heat exchangers is also derived to describe the mass transfer in these hollow fiber cross-flow contactors. To validate the numerical model as well as the analytical expression experimentally, carbon dioxide absorption was carried out in cross-flow membrane contactors using water as a solvent. The main

aim of the study was to study the performance of cross-flow membrane contactors using a numerical model based on first principles; hence the experiments were performed with water on the fiber side and gas on the shell side. The liquid on the fiber side also helps in the visual inspection of fiber for possible wetting of the membrane fibers. However, it should be noted that passing the phase with the controlling mass transfer resistance on the shell side gives a better overall performance.

2. Application of heat transfer analogy

The literature on the mathematical analysis of cross-flow heat exchangers is mainly focused on the calculation of mean temperature difference in single-pass and multi-pass heat exchangers for various shell-side mixing patterns [9,10]. In the present work, shell-side fluid is considered completely mixed and the fiber-side fluid is assumed to consist of independent streams between which there is no mixing. The derivation of the analytical expression is carried out for the case of single-pass cross-flow membrane contactor. Since the shell-side fluid is considered as completely mixed in the direction normal to its flow, there is no concentration gradient normal to the flow of fluid. The average dimensionless outlet concentration of the shell-side fluid (fluid '1') is given by Eq. (1); using the overall mass balance the average concentration of the fiber-side fluid can also be calculated. The mathematical derivation of the outlet concentration of the shell-side fluid is given in Appendix A:

$$\Theta_{1,\mathrm{ex}} = 1 - \exp\left[\frac{mQ_2}{Q_1}\left(\exp\left(\frac{-KA}{Q_2}\right) - 1\right)\right] \tag{1}$$

3. Numerical model

In membrane gas–liquid contactors, the gas phase flow can change considerably due to absorption. This is especially true when the gas stream contains a considerable amount of a highly soluble solute gas and particularly important at higher removal rates. In multi-component absorption processes, the higher absorption of one component results in an increase in the partial pressure of the slower absorbing component resulting into increased driving force for slower absorbing component. This inverse coupling of the concentration differences leads to a complex situation where the direct application of the cross-flow heat exchanger analogy may lead to erroneous results. Moreover, when the absorption of one (or more) gaseous component is enhanced by a chemical reaction, the heat transfer analogy is no longer valid. Hence it is necessary to develop a numerical model that takes into account the changes in the gas flow rate as well as variations in the concentration driving force. The present numerical model is based on the following assumptions:

1. steady state and isothermal operation (non volatile liquid phase);
2. laminar flow within the fiber;
3. the membrane pores are gas filled;
4. the shell-side flow can be described by a number of ideally mixed cells in both directions;
5. pitch and placing of the fibers are well defined and uniform.

Using above assumptions, the steady state mass balance in the fiber for the transport of component '*j*' can be written as:

$$v_z\frac{\partial C_j}{\partial z} = D_j\left[\frac{1}{r}\frac{\partial}{\partial r}\left(r\frac{\partial C_j}{\partial r}\right)\right] \tag{2}$$

In arriving at Eq. (2), the diffusion in axial direction was neglected and axis-symmetry of the hollow fiber was assumed. Since the liquid flow inside the fiber is laminar, the velocity profile in the radial direction is given by

$$v_z = 2V_{\mathrm{L}}\left(1 - \left(\frac{r}{R}\right)^2\right) \tag{3}$$

This set of partial differential equations need to be solved for each component with the initial condition:

$$\text{At } z = 0, \quad C_j = C_{j,\mathrm{in}} \tag{4}$$

At the centre of the fiber the concentration profile is symmetric which results in the boundary condition equation (5):

$$\text{At } r = 0, \quad \left(\frac{\partial C_j}{\partial r}\right) = 0 \quad (0 \quad z \quad L) \tag{5}$$

At the gas–liquid interface i.e. the membrane wall mass transfer of the solute component occurs, which is described by Eq. (6):

$$\text{At } r = r_{in}, \quad -D_j\left(\frac{\partial C_j}{\partial r}\right) = k_{\mathrm{ext}}(C_{j,\mathrm{G,bulk}} - C_{j,\mathrm{G,i}}) \quad (0 \quad z \quad L) \tag{6}$$

where 'k_{ext}' is the overall mass transfer coefficient obtained by combining membrane wall and gas phase transport resistance respectively. For a non-volatile liquid phase component flowing through the fiber, the boundary condition at the gas–liquid interface is given by Eq. (7):

$$\text{At } r = r_{in}, \quad D_j\left(\frac{\partial C_j}{\partial r}\right) = 0 \quad (0 \quad z \quad L) \tag{7}$$

A typical operation of a cross-flow membrane contactor is illustrated in Fig. 2 with liquid flowing through the hollow fibers and gas flowing on the shell side. The solvent at the entrance of the cross flow membrane contractor can either be fresh, unloaded solution or partially saturated with the solute, whereas at the outlet of the liquid stream the solvent has an increased solute loading. Thus there is a gradual decrease in the driving force along the length of fiber. This results into higher absorption rates at the liquid entrance side as

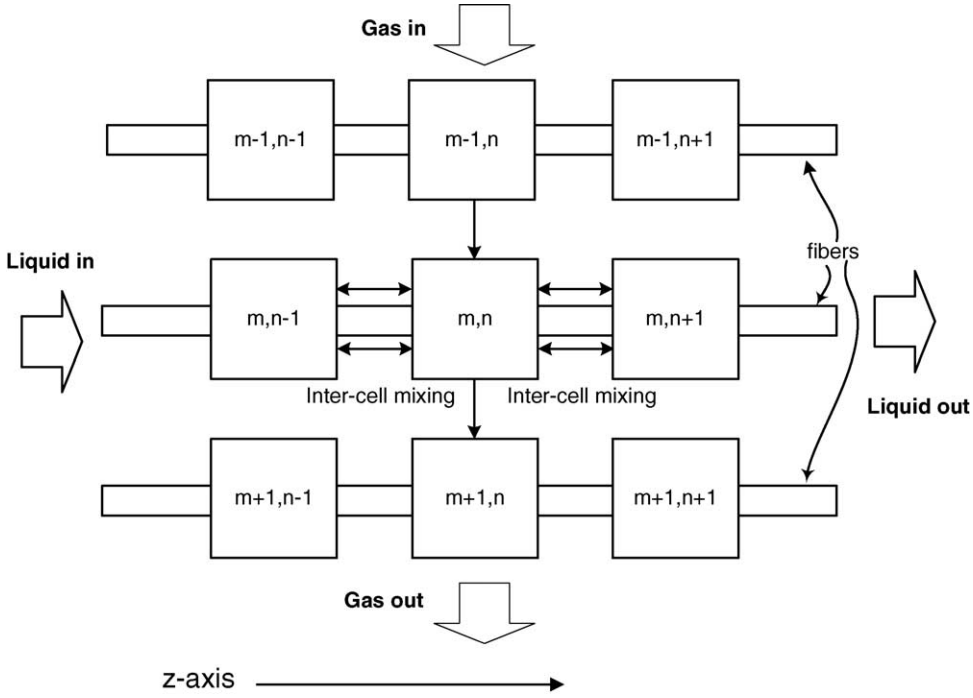

Fig. 2. Cross-flow membrane contactor and cell arrangement for shell-side flow.

compared to the liquid outlet side. As a consequence the drop in shell-side solute concentration, in the direction of gas flow, is deeper near the liquid entrance as compared to the drop in the shell-side solute concentration near the liquid exit. This effect is significant when the concentration of the solute in the gas stream is high and/or the solubility is high, thus resulting into the higher removal rates in the membrane contactor. To take this effect into account, the shell-side stream is divided into a number of unit cells. This cell method preserves the concentration gradients of the gas and liquid phase in both directions. The applied cell arrangement is shown in Fig. 2. Each cell is assumed to be completely, ideally mixed and there is no back mixing in the direction of the flow. The number of cells in the direction of the flow represents the well known "CSTR in series" model. Note that in the direction perpendicular to the gas flow mixing takes place between the adjacent cells. A solute balance over a single cell gives following equation:

$$Q_{\mathrm{G}\,m-1,n}C_{\mathrm{G}\,m-1,n} - Q_{\mathrm{G}\,m,n}C_{\mathrm{G}\,m,n} = Q_{\mathrm{L}\,m,n}\left(C_{\mathrm{L}\,m,n} - C_{\mathrm{L}\,m,n-1}\right) = A_{m,n}J_{m,j} \quad (8)$$

where '$A_{m,n}{}'$' and '$J_{m,n}$' are the mass transfer area and mass transfer flux (from shell-side to fiber-side) within the cell (m, n), respectively.

Based on this mass balance for a single cell the solute outlet concentration and the gas outlet flow rate can be calculated for every cell by an iterative method. Ideal gas law was assumed to calculate change in volumetric flow rate. To initiate the calculation, the gas concentration, gas flow rate and liquid concentration were assumed to be uniform over the inlet of the module. The composition and gas flow rate leaving the row of cells were stored and used as inputs for the corresponding cells in next row. At the last row, the average outlet concentration was calculated by the mixing cup method.

Three different stages of mixing can be defined and were used for the mixing between the adjacent cells in this model. First option assumes no mixing between the adjacent cells, so the entire row of the gas moves up to the next segment. This rule results into maximum concentration gradient on the shell side. The second option is that the gas leaving one segment is completely mixed (along z-axis) before entering next segment. The third option is an intermediate case with respect to the first two alternatives. In this case, the mixing between the adjacent cells perpendicular to the flow direction is calculated using Fick's law (see Fig. 2):

$$J_{\text{inter-cell mixing}}(m,n) = -E\left(\frac{\partial C_{j,\mathrm{s}}}{\partial z}\right) \quad (9)$$

where 'E' is the dispersion coefficient between the adjacent cells in the direction perpendicular to the flow. To get an impression of actual shell-side dispersion coefficients, in the direction of flow and in the direction normal to the flow, these parameters were determined in separate experiments using RTD analysis. The details of these RTD experiments and results are presented elsewhere [3] and are used in this study.

The complete solution of the model was obtained by solving of a system of non-linear parabolic partial differential equations (Eqs. (2)–(9)), subjected to specified initial and boundary conditions, simultaneously with the shell-side mass

Table 1
Module specifications

Module	Fiber type	Length (m)	Width (m)	Height (m)	No. of fibers	Voidage	Pitch	A (m^2)
I	PP	0.1	0.1	0.1	4900	0.615	1.45	0.924
II	PP	0.1	0.04	0.04	400	0.8	2.0	0.074

balance. The final set of the partial differential equations were discretised using the implicit second order scheme based on the Baker and Oliphant [1] method and solved using a technique similar to the one described by Versteeg et al. [11]. The concentration profiles on the shell side as well as on the fiber side were obtained as a solution.

4. Experimental

4.1. Material

Double distilled water was used as an absorption solvent. Carbon dioxide and nitrogen used in the experiments were of 99.99% purity. Owing to the commercial availability and the high hydrophobic nature of polypropylene as a membrane material, it was decided to use an Accurel Q3/2 polypropylene hollow fiber (outside diameter = 1000 μm; inside diameter = 600 μm; maximum pore size = 0.64 μm) for module construction. Two modules were used in the experiments. The details of the modules are given in Table 1.

Module I was provided by TNO-MEP, Apeldoorn, and module II was specifically constructed for the present work. The details of the modules are shown in Fig. 3a and b. Both modules had PVC shell housing. Fibers in both modules were arranged in square pitch. For construction simplicity, the shell housing of module II was kept circular with an internal diameter of 5 cm. To make the shell-side flow area rectangular in cross section, a rectangular opening was cut from the circular shell and the concave volume of the shell was filled with the epoxy resin. To arrange the fibers uniformly the tube-sheets of the module II were drilled with 1.2 mm precision drill with square pitch. The fibers were then woven through the tube sheets. Once all fibers were woven, a liquid epoxy resin (slow setting) was poured on the tube sheet to fill the gaps between the fibers. Sufficient time (12 h) was allowed to cure the epoxy. The procedure was repeated until the desired length of the epoxy glue was obtained. The same procedure was used to pot the other end of the module. In both modules the length of the potting was more than 5 cm. This ensures that the potting length on the liquid entry side provides sufficient distance ($>10d_{in}$) for the laminar liquid flow profile inside the fiber to be fully developed, before it contacts the gas. Uniform flow distribution on the shell side is important to prevent the mal-distribution and dead zones formation. To achieve uniform flow distribution on the shell-side, fluid was passed through an area-reducer filled with glass wool as packing material.

4.2. Method

The experimental set-up to study the physical absorption of carbon dioxide in the cross-flow membrane modules is shown in Fig. 4. A continuous mode of gas–liquid contacting operation was used during the experiments. The liquid was passed through the fibers and gas was passed through the shell side. The solvent (water) was fed from a gear pressure pump via a flow controller. The water used in the experiments was degassed before usage by nitrogen bubbling in a separate apparatus. The water was passed through the

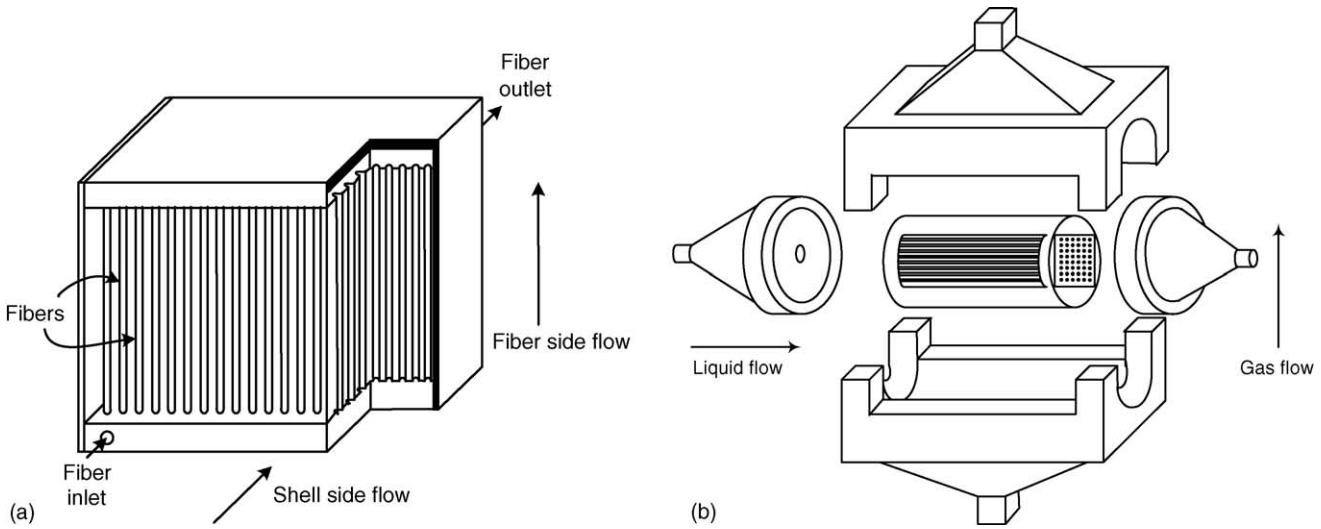

Fig. 3. (a) Cross-flow membrane module I; (b) cross-flow membrane module II.

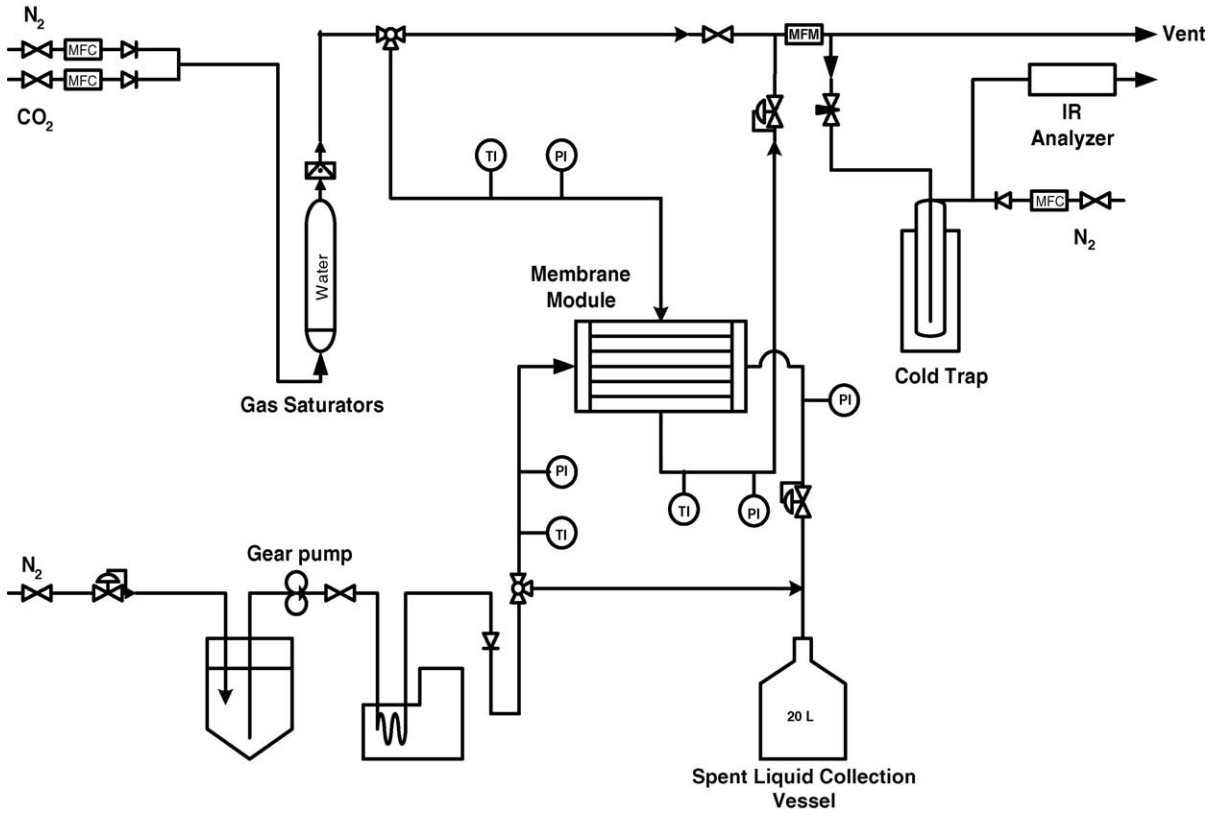

Fig. 4. Cross-flow membrane module experimental set-up.

heat exchanger to maintain the desired temperature before passing to the hollow fiber membrane module. The upstream solvent pressure was controlled using a high-precision back-pressure controller valve. In all experiments, sufficient gas pressure was maintained in the contactor before starting the liquid flow as the absence of the gas pressure may result in the wetting of the fiber. The liquid inlet and liquid outlet pressures were measured separately using digital pressure indicators. The liquid inlet was also fitted with a digital thermometer to monitor the liquid inlet temperature. The average velocity of the liquid through the fibers was measured by collecting a calibrated amount of sample in a fixed period of time.

The shell-side gas flow was adjusted using Brooks precision mass-flow controllers. All mass flow controllers were calibrated by means of a gas flow meter and/or soap film meter. Nitrogen and carbon dioxide were premixed to a desired concentration using mass flow controllers and fed to the contactor after saturating the gas stream with water vapor. The shell-side pressure was controlled using a 5866-Brooks digital pressure controller. During all the experiments the liquid-side pressure was kept higher than the shell-side gas pressure to avoid the bubbling of gas. The gas inlet and gas outlet pressure were measured separately using digital pressure indicators. The gas inlet and gas outlet were also equipped with digital thermometers to monitor the temperatures. It is important to know both inlet and outlet temperatures of the gas stream in order to check any cooling effect which might result into a change in the volumetric gas flow rate. The carbon dioxide concentration in the feed and outlet gas streams of the contactor was measured using Maihak Infrared carbon dioxide analyzers of different ranges depending on gas composition (0–5 and 0–15%). The experiments were carried out using either pure carbon dioxide or mixed streams of nitrogen and carbon dioxide. The samples of the gas stream were adjusted by dilution with calibrated amounts of nitrogen in order to arrive at the concentration range required by the infrared analyzer. The carbon dioxide absorption flux and liquid average outlet concentration were calculated by an overall mass balance over the reactor:

$$\langle J_{CO_2} \rangle = \frac{Q_{G,in}C_{G,in} - Q_{G,ex}C_{G,ex}}{A} \tag{10}$$

In membrane gas–liquid contactors, although gas is only in contact with liquid at the pore mouths, total membrane area needs to be used as the mass transfer area [8]. Hence, in calculating the carbon dioxide absorption flux using Eq. (10), total physical membrane area is used. The liquid outlet concentration can be calculated by taking solute mass balance over the contactor and is given by Eq. (11):

$$C_{L\,out} = \frac{Q_{G,in}C_{G,in} - Q_{G,ex}C_{G,ex}}{Q_L} \tag{11}$$

Since the infrared analyzer gave carbon dioxide concentration in terms of volume percentage, it was possible to

Table 2
Experimental details

Volume (% CO_2)	CO_2 (mol m^{-3})	Module arrangement	Average pressure (atm)	Temperature (K)	Gas residence time (s)	Liquid residence time (s)
2.5	1.20	Single unit type: II	1.15	293	14.36	1.0–1.5
30.0	14.62	Single unit type: II	1.18	295	25.6–8.8	1.0–10.0
87.5	51.69	Single unit type: II	1.43	295	26.6	1.1–16.7
100.0	45.36	Single unit type: II	1.10	295	52.1	0.9–3.3
70.0	39.33	Single unit type: I	1.36	295	3.7	1.1–9.1
30.0	14.13	Single unit type: I	1.14	295	4.5	1.1–7.7
70.0	34.82	Two type I units: co-current	1.20	294	6.42	1.2–8.3
70.0	34.82	Two type I units: counter-current	1.20	294	6.42	1.3–10.0

calculate both the volumetric gas flow rate and the molar concentration of carbon dioxide by mass balance. In all experiments the gas flow rate was kept sufficiently low so that the outlet gas flow rate and molar concentration of the carbon dioxide were significantly lower than the inlet conditions. All the experiments were carried at ambient conditions. The detailed experimental conditions are given in Table 2. The solubility of carbon dioxide in water at experimental conditions was taken from Versteeg and van Swaaij [12].

5. Results and discussions

5.1. Absorption experiments with single module

Experiments were carried out in module II to study the influence of various operating parameters such as gas-velocity, liquid-velocity and CO_2 partial pressure on the module performance. In all experiments the gas residence time in the membrane module was kept considerably high to get a significant change in the gas phase concentration. Initial experiments were carried out using very low percentage of the carbon dioxide in the inlet gas stream and low rates of removals in order to avoid large changes in the volumetric gas flow rate due to absorption. Fig. 5 shows the liquid phase and gas phase outlet concentrations of carbon dioxide for the absorption of carbon dioxide into water as a function of the liquid velocity through the fiber. The experiments were carried out using 2.5% (1.2 mol m^{-3}) carbon dioxide in the inlet gas stream with constant gas inlet flow rate of 0.65 l/min. It can be seen from the figure that with increase in the liquid velocity both liquid and gas outlet concentrations decrease. The numerical model using third mixing option and the heat transfer analogy (HT) predictions of outlet gas and liquid concentrations are both in good agreement with experimental results. The effect of mixing option in the numerical model was found to be negligible due to the flat shell-side concentration profile. It is important to note that in these experiments CO_2 removal was always less than 15%. Moreover, the change in volumetric flow rate of the gas was very small (less than 0.5%) and allowed to be neglected.

To analyze the effect of a change in the volumetric flow rate of the gas stream, experiments were carried out at relatively high removal rates and using a gas stream containing a high percentage of carbon dioxide. Figs. 6 and 7 show the gas and liquid outlet concentrations for the absorption of 30% (14.62 mol m^{-3}) and 87.5% (51.69 mol m^{-3}) carbon dioxide in module II, respectively. The experiments were carried out at constant inlet gas flow rate of 0.38 l/min and 0.36 l/min for absorption of 30 and 87.5% carbon dioxide, respectively. It can be seen from the graphs that both gas phase and liquid phase outlet concentration are strong functions of the liquid velocity. Both liquid and gas phase outlet concentrations as predicted by the numerical model are in good agreement with experimental results. However, the gas phase concentrations predicted by heat transfer analogies (HT) are lower from the experimental results and this deviation increases

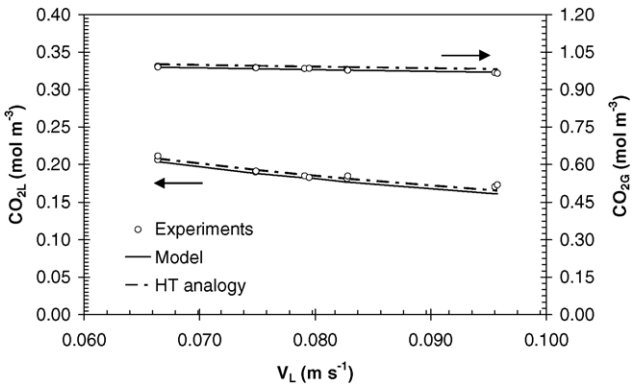

Fig. 5. Carbon dioxide (2.5%) absorption in module II for constant inlet gas flow rate of 0.65 l/min.

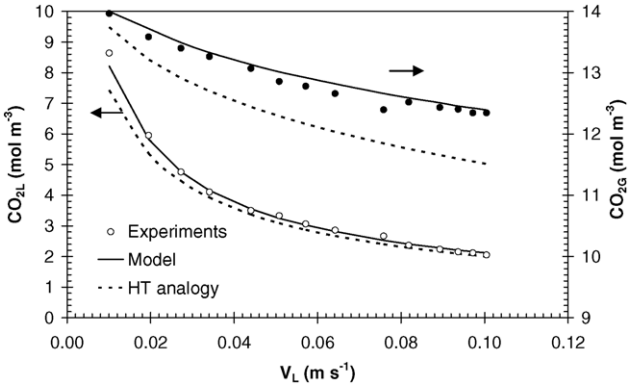

Fig. 6. Carbon dioxide (30%) absorption in module II for constant inlet gas flow rate of 0.38 l/min.

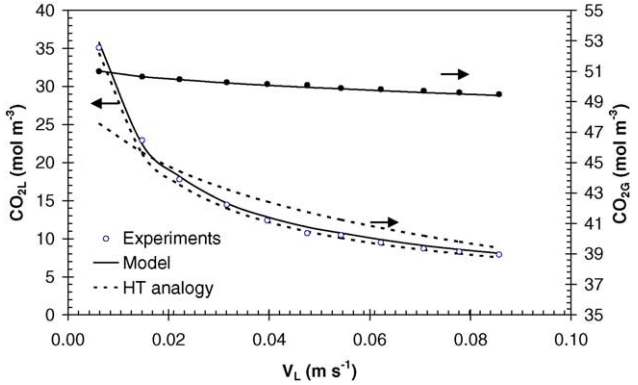

Fig. 7. Carbon dioxide (87.5%) absorption in module II for constant inlet gas flow rate of 0.36 l/min.

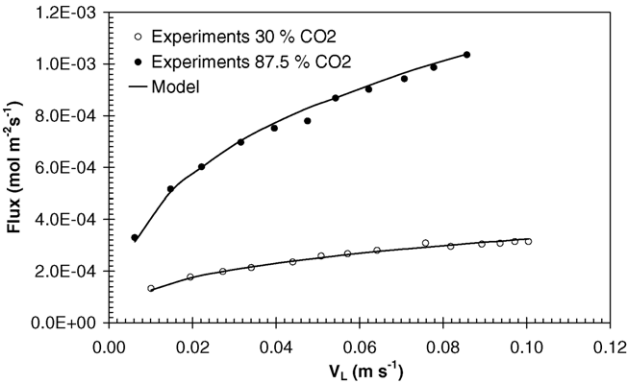

Fig. 9. Effect of liquid velocity on the absorption flux (module II) for constant inlet gas velocities ($V_G = 1.6 \times 10^{-3}$ m s^{-1} for the absorption of 30% CO_2; $V_G = 1.5 \times 10^{-3}$ m s^{-1} for the absorption of 87.5% CO_2).

with the liquid velocity. As a result of the lower predicted gas phase concentration and hence lower predicted mass transfer driving force, the liquid outlet concentrations calculated by heat transfer analogy (HT) are also lower as compared to the numerical model. In general, the transfer of moles from gas phase to the liquid phase results into decrease in the gas phase volumetric flow rate as well as decrease in the gas phase solute concentration. However, the analytical expression based on heat transfer analogy is derived assuming the constant volumetric flow rate for both gas and liquid phase and only takes into account the change in the solute concentration. As the solute concentration in the gas-phase and the removal rate increase, the decrease in the volumetric flow rate is more pronounced than the decrease in the solute concentration. In present case, the change in volumetric gas flow rate was more than 10% for both conditions. In addition, percentage removal as well as change in gas flow rate increases with the liquid velocity and hence the deviation in the prediction of gas phase outlet concentration by heat transfer analogies also increases with the liquid velocity. In the asymptotic case of a pure gas and isobaric operation only the volumetric flow rate will change. Fig. 8 shows the absorption of pure carbon dioxide in module II for constant inlet gas flow rate of 0.18 l/min. Thus when solute gas phase concentration is relatively high and removal rate is significant, heat transfer analogies based on the constant flow rate cannot be used to estimate the module performance. Fig. 9 shows the absorption flux as a function of the liquid velocity at constant gas velocities (1.6×10^{-3} m s^{-1} for the absorption of 30% carbon dioxide and 1.5×10^{-3} m s^{-1} for the absorption of 87.5% carbon dioxide). Fig. 10 shows the absorption flux as a function of the gas velocity at constant liquid velocity of 0.055 m s^{-1}. The absorption flux is a strong function of the liquid velocity whereas the gas velocity has almost a negligible influence on the absorption flux. This confirms the fact that in the case of physical absorption of a sparingly soluble gas, the controlling mass transfer resistance lies on the liquid side.

Similar results were obtained for absorption of carbon dioxide using the larger module I. The results are presented in Figs. 11 and 12. The gas flow rate during the experiment was kept constant at 16.1 l/min for the absorption of 70% (39.33 mol m^{-3}) carbon dioxide and at 13.3 l/min for the absorption of 30% (14.13 mol m^{-3}) carbon dioxide. The percentage removal of carbon dioxide in both experiments was very low, typically below 8%, due to the low gas residence

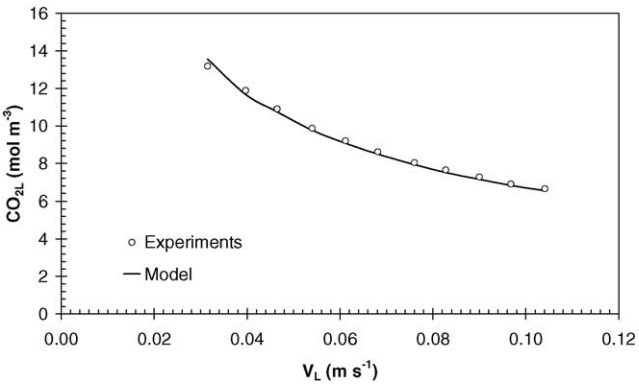

Fig. 8. Absorption of pure carbon dioxide in module II for constant inlet gas flow rate of 0.18 l/min.

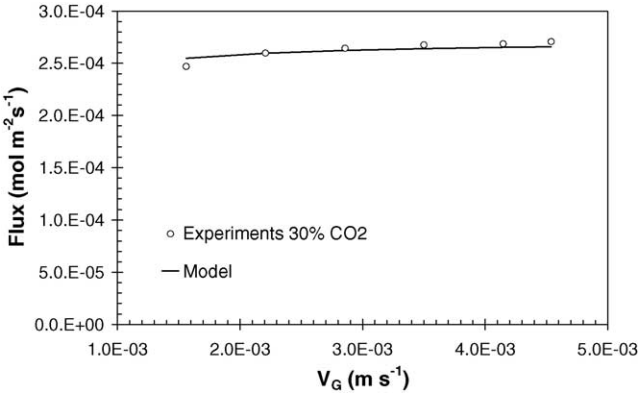

Fig. 10. Effect of gas velocity on the absorption flux (module II) for constant liquid velocity ($V_L = 0.055$ m s^{-1}).

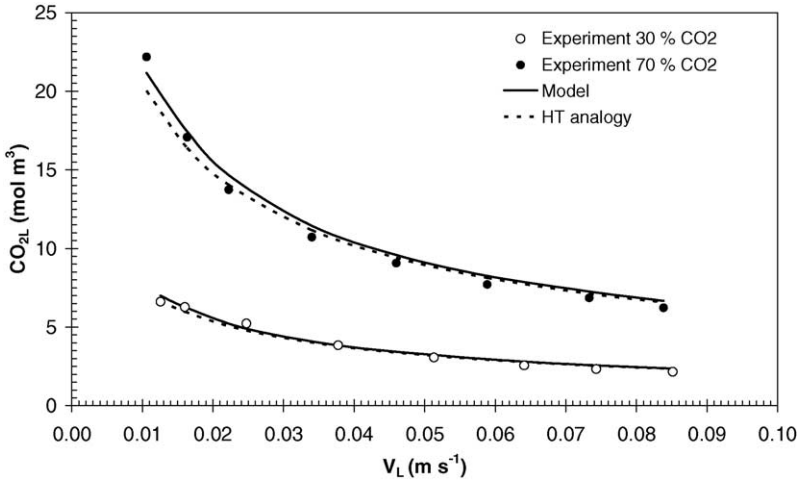

Fig. 11. Effect of liquid velocity on the liquid outlet concentration for absorption in module I for constant inlet gas flow rate (Q_G = 16.1 lit/min for the absorption of 70% CO_2; Q_G = 13.3 lit/min for the absorption of 30% CO_2).

time. Hence, the model as well as the heat transfer analogy predictions of gas outlet concentrations are in good agreement with the experiments.

5.2. Absorption experiments with two modules in series

For any set of concentrations, the average concentration difference between the two phases is higher for counter-current operation compared to the co-current or cross-flow arrangement. Therefore the performance of the counter-current flow arrangement is generally assumed to be better for processes involving equilibria. An overall counter-current and/or a co-current pattern can be realized by cascading two or more cross-flow modules while maintaining the advantages of cross-flow operation at each stage. The co-current and counter-current flow arrangement is shown in Fig. 13.

Absorption of 70% (34.82 mol m^{-3}) carbon dioxide at constant inlet gas flow rate of 9.35 l/min was carried out to study the effect of cascading of two cross-flow modules. The results are shown in Fig. 14. The figure shows the effect of the liquid velocity on the absorption flux for a cascade of two modules. Hardly any difference is obtained between these two cases. This can be attributed to the relatively small percentage removal (less than 20%) which is in line with the observations made by Wang and Cussler [13]. At smaller removal rates, the change in inlet and outlet concentrations is relatively small and thus the average concentration difference between the two phases is unaffected by the co-current or counter-current mode of operation. The numerical model also indicates no significant difference in the performance of the stack of two modules in co-current or counter-current flow arrangement. However, a closer look on the numerical model indicates that, as expected, at higher velocities the flux obtained in the counter-current flow is slightly higher than in the co-current flow arrangement. Differences will be more pronounced for stacks of more modules and/or at higher removal fractions. It should be noted that in the case of counter-current operation for the model, the exit gas concentration and the gas

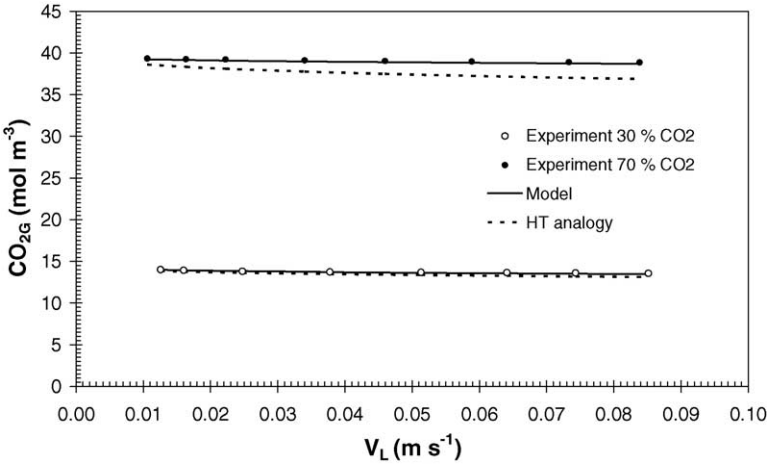

Fig. 12. Effect of liquid velocity on the gas outlet concentration for absorption in module I for constant inlet gas flow rate (Q_G = 16.1 lit/min for the absorption of 70% CO_2; Q_G = 13.3 l/min for the absorption of 30% CO_2).

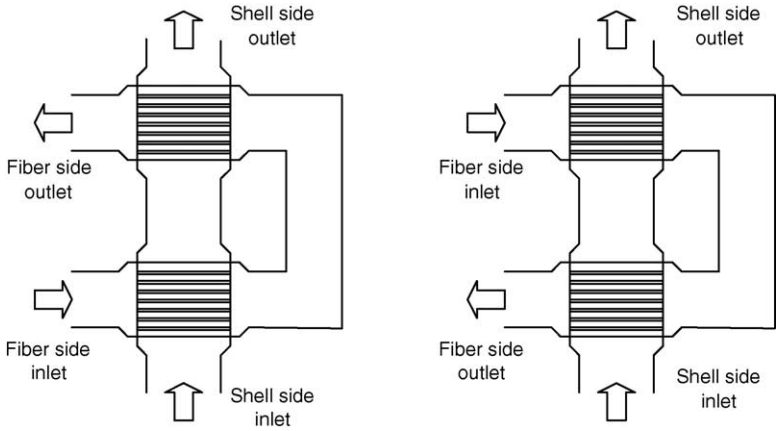

Fig. 13. Co-current and counter-current arrangement of two modules in series.

flow rate must be guessed to start the calculations. In actual model, the uniform feed concentration and flow rate would result in a concentration and flow gradient in the gas leaving the final segment. Thus in principle gas outlet concentration and flow gradient must be guessed to start the calculation, which results into complex and tedious calculation. To make the calculation routine easy, the uniform gas outlet concentration and uniform gas outlet flow for each module were guessed. Thus the calculations result in concentration and flow gradient in the incoming feed even though the actual feed has no gradient. The mixing cup concentration of the incoming feed was then compared with the known feed concentration and guess of exit concentration and flow rate were adjusted if necessary.

5.3. *Performance analysis of cross-flow membrane module with the numerical model*

The developed numerical model is a useful tool for calculating the two-dimensional concentration profiles on the shell as well as on the fiber side and thus calculating the local concentration driving force. The understanding of the driving force and concentration profiles within the modules is useful for optimizing the flux in the module and thus

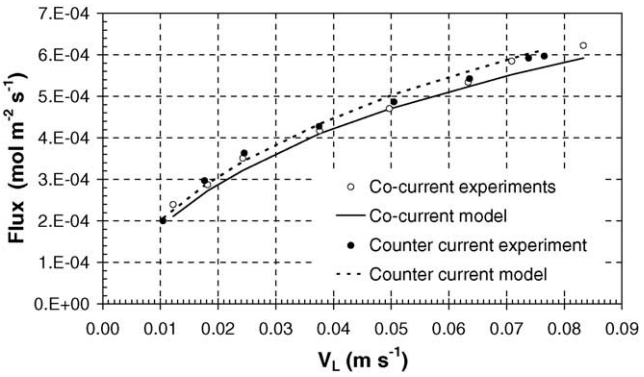

Fig. 14. Effect of module arrangement on the absorption flux for constant inlet gas flow rate of 9.35 l/min.

selecting the ideal operating conditions. Numerical simulations were carried out for the absorption of carbon dioxide into fresh unloaded water using TNO modules (module type I) to study the effect of operating conditions on the shell-side concentration profiles. The shell-side flow was divided into 20 cells along the length of the fiber and 70 cells (equal to the number of fibers; cell dimension 5 mm × 1.42 mm) in the direction of gas flow and no mixing between the adjacent cells was assumed. In this way maximum variation in the shell-side gas concentration over the module was obtained. Fig. 15a–c shows the shell-side gas concentration for three different values of percentage removals.

When percentage removal is 70%, most of the solute is removed from the gas phase. It can be seen from Fig. 15a that the drop in the shell-side solute concentration in the direction of gas flow is very sharp at the liquid entrance as compared to the liquid exit. This is because the driving force is the largest in the module where gas first meets the clean unloaded liquid. However, at the liquid exit, the liquid is partially loaded with the solute and hence the decrease in the shell-side solute concentration near the liquid exit is smaller. The combination of these effects results into reversal of the concentration driving force gradient along the length of fiber near the gas exit. The shell-side concentration profile is also useful in identifying less efficient/dead zone for mass transfer. The region near the liquid entrance and the gas exit has very low gas concentration and therefore is less efficient in the mass transfer process. In such cases, local reversal of the liquid flow direction or the installation of baffles perpendicular to gas flow to enhance the mass transfer in less efficient zones will improve the overall driving force.

By increasing the gas flow rate, the percentage removal as well as the shell-side gas concentration gradient decreases as shown in the case of 20 and 10% removal (refer Fig. 15b and c). At very low removal rates, there would be hardly a gradient in the shell-side gas concentration. In this case, the liquid outlet concentration and the mass transfer flux can be calculated by a simple mass balance across the whole module.

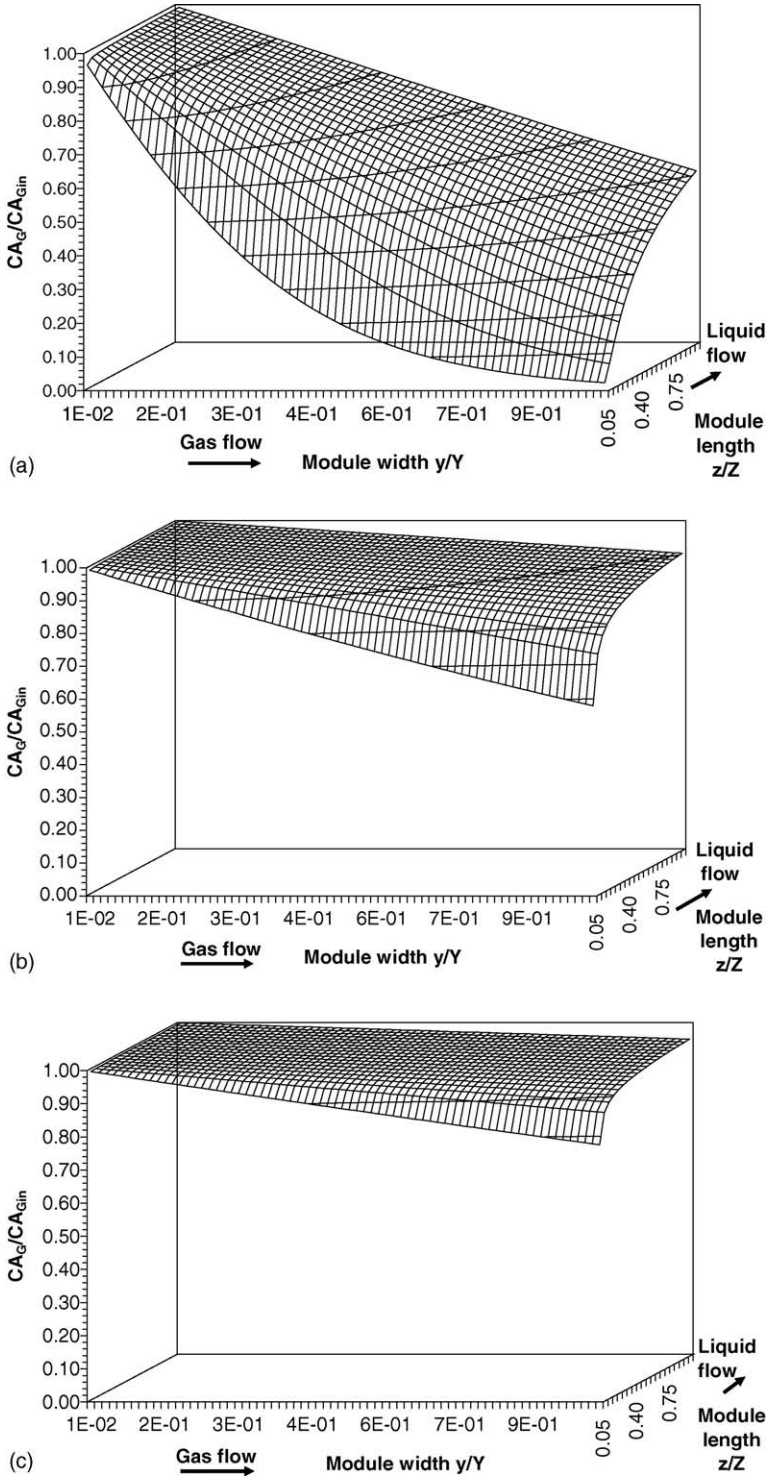

Fig. 15. (a) Shell-side concentration profile at 70% removal for constant inlet gas velocity of 2×10^{-3} m s^{-1} and liquid velocity of 0.125 m s^{-1}. (b) Shell-side concentration profile at 20% removal for constant inlet gas velocity of 1×10^{-2} m s^{-1} and liquid velocity of 0.125 m s^{-1}. (c) Shell-side concentration profile at 10% removal for constant inlet gas velocity of 2×10^{-2} m s^{-1} and liquid velocity of 0.125 m s^{-1}.

The sensitivity of the numerical model with respect to the shell-side mixing rules was also analyzed. Numerical simulations were carried out for the absorption of 30–70% carbon dioxide–nitrogen mixture into fresh unloaded water using the TNO module at different operating conditions to get different removal rates. Fig. 16 shows the percentage deviation in the outlet gas concentration obtained between complete mixing on shell side and no mixing on shell side as a function of removal percentage. The percentage error is defined as the relative difference between the outlet concentrations

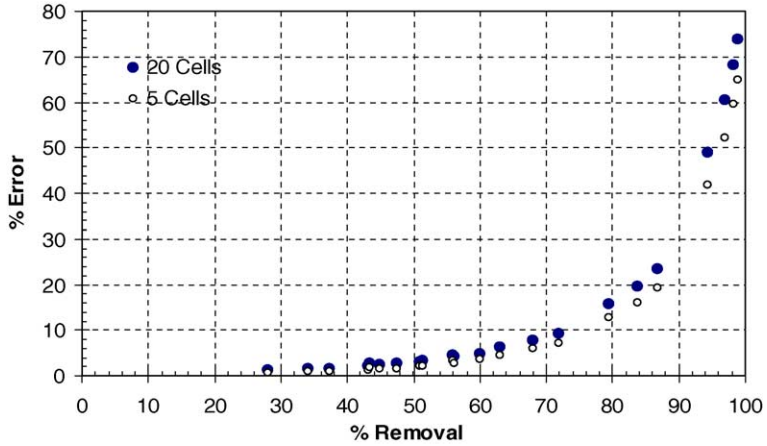

Fig. 16. Effect of shell-side mixing on the gas outlet concentration (% error is defined as $100 \times (C_{G\,\text{out-single cell}} - C_{G\,\text{out-}'n'\,\text{cells}})/C_{G\,\text{out-single cell}}$).

obtained with complete mixing on shell side i.e. using a single cell and the outlet concentration obtained using multi-cells with no mixing among the cells. It can be seen from the figure that at low percentage of removal both mixing patterns give the same outlet concentrations. However, at higher percentages of removal the deviation in outlet concentration increases substantially. This is because at a higher percentage of removal, the concentration gradient on shell side is steep. Hence the number of cells and mixing pattern has a significant effect on the performance of the module. At low percentage of removal the shell-side concentration profile is flat and the mixing between the cells becomes unimportant. The positive values of error indicate that the outlet concentration obtained using multi-cells is much lower as compared to that obtained using single cell. Thus indicating that the 'no-mixing' on shell-side using multi-cells gives better performance as compared to that of the 'complete-mixing' rule using a single cell on the shell-side.

6. Conclusion

In the present study, physical gas absorption in a rectangular cross-flow membrane gas liquid contactor is discussed in detail. Experiments were carried out to study the effect of various parameters such as gas and liquid flow rates, solute concentration in the feed stream on the performance of the rectangular cross-flow membrane gas–liquid contactors. The possibility of application of the cross-flow heat exchanger analogy in the limiting cases to the cross-flow membrane gas–liquid contactor is also explored. At low removal rates and/or low solute concentrations in the feed stream the experimental results match very well with the predictions of heat transfer analogies. However, at the higher percentage of removals and at higher solute concentrations the change in the volumetric flow is significant and heat transfer analogies can no longer be used to predict the performance of the cross-flow gas–liquid membrane contactor. To predict the performance of the cross-flow membrane contactor in such cases a detailed mathematical model is developed. The predictions of the developed numerical model are in good agreement with the experimental results. Three different mixing patterns namely, complete mixing, no mixing and dispersive mixing on the shell side were considered. The numerical simulations show that the type of shell-side mixing is important at high percentages of solute removal. At low percentage of removal all mixing rules give same results. At higher percentage of removal no mixing on the shell side gives better performance. The model developed can be used in design and optimization of cross-flow membrane modules for (multi-component) membrane gas absorption processes.

The strong dependence of the absorption flux on the liquid velocity confirms the observation that in the case of physical absorption controlling mass transfer resistance lies on the liquid side. The experimental study of co-current and counter-current arrangements for stack of two modules showed no significant difference in the performance of the module. This, however, can be attributed to the small percentage of removal obtained in the lab scale modules. Nonetheless, the detailed numerical simulations indicate that at higher rate of removal overall counter-current arrangement gives better performance.

Acknowledgement

This research is part of the research program performed within the Centre for Separation Technology (CST), which is a co-operation between the Netherlands Organization for Applied Scientific Research (TNO) and the University of Twente. We acknowledge Benno Knaken and Wim Leppink for the construction of the experimental set-ups and Irene Gootje for administrative support.

Appendix A. Derivation of analytical expressions based on heat transfer analogy

Following assumptions are made while deriving the heat transfer analogy for the cross-flow membrane contactor:

1. steady state and isothermal operation (non-volatile liquid phase);
2. no chemical reaction;
3. the changes in flow rates are very small and can be neglected;
4. overall mass transfer coefficient and distribution coefficient are constant over the module;
5. the pitch and placing of the membrane fibers are uniform and similar to that of the heat transfer equipments.

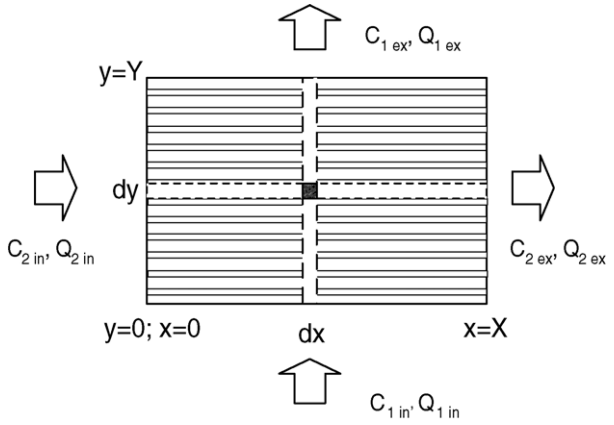

Fig. A.1. Cross-flow hollow fiber membrane contactor: application of heat transfer analogy.

Let the shell-side fluid Q_1 be flowing in y-direction and is completely mixed (refer Fig. A.1). The fiber-side fluid Q_2 is unmixed and is flowing in x-direction. Since the mixing on the shell side is assumed to be complete, C_1 is a function of y only and C_2 is a function of both x and y. Consider the strip of width 'dy' at y. The fluid flowing across this strip is having a constant concentration C_1, while the fluid flowing along the strip is unmixed and its varying concentration C_2 is determined by

$$\frac{\partial C_2}{\partial x} = \frac{KY}{Q_2}(mC_1 - C_2) \tag{A.1}$$

where 'm' is distribution coefficient. Eq. (A.1) subject to boundary condition:

$$C_2 = C_{2,\text{in}} \text{ at } y = 0 \tag{A.2}$$

The outlet concentration from the strip is given by

$$\frac{(mC_1 - C_{2x,y})}{(mC_1 - C_{2,\text{in}})} = \exp\left(\frac{-KXY}{Q_2}\right) \tag{A.3}$$

where K is overall mass transfer coefficient of the membrane contactor. In the case of physical absorption into a liquid flowing through a fiber, the overall mass transfer coefficient can be approximated to the fiber-side mass transfer coefficient and is given by Eq. (A.4) [8]:

$$K = 1.62D^{2/3}\left(\frac{V_L}{2Lr_{in}}\right)^{1/3} \tag{A.4}$$

where V_L is the average liquid velocity through the fiber.

The total mass transfer in the strip to the mixed shell-side fluid is

$$Q_2(C_{2,\text{in}} - C_{2x,y})\frac{\mathrm{d}y}{Y} = Q_1\,\mathrm{d}C_1 \tag{A.5}$$

Using Eqs. (A.5) and (A.3)

$$Q_2(mC_1 - C_{2,\text{in}})\left(\exp\left(\frac{-KXY}{Q_2}\right) - 1\right)\frac{\mathrm{d}y}{Y} = Q_1\,\mathrm{d}C_1 \tag{A.6}$$

The product 'XY' is the total mass transfer area of the module. Rearranging and integrating Eq. (A.6) from 0 to X and using boundary conditions at $x = 0$, $C_1 = C_{1,\text{i}}$ and at $x = X$, $C_1 = C_{1,\text{ex}}$, the final outlet concentration of the shell-side fluid can be given by

$$\Theta_{1,\text{ex}} = \frac{(mC_{1,\text{in}} - mC_{1,\text{ex}})}{(mC_{1,\text{in}} - C_{2,\text{in}})} = 1 - \exp\left[\frac{mQ_2}{Q_1}\left(\exp\left(\frac{-KA}{Q_2}\right) - 1\right)\right] \tag{A.7}$$

Nomenclature

A	area [m^2]
C	concentration [mol m^{-3}]
D	diffusivity [$m^2\ s^{-1}$]
E	dispersion coefficient [$m^2\ s^{-1}$]
J	flux [mol $m^{-2}\ s^{-1}$]
K, k	mass transfer coefficient [m s^{-1}]
L	length [m]
m	distribution coefficient [–]
Q	flow rate [$m^3\ s^{-1}$]
r	radius [m]
v	velocity [m s^{-1}]
X	x-dimension of module [–]
Y	y-dimension of module [–]
z	length [m]

Greek letter

Θ	dimensionless concentration

Subscript

bulk	bulk phase
ex	exit
ext	external
G	gas
i	interface
in	inlet/inner
j	component 'j'
L	liquid

t	tube side
s	shell side
z	local value
1	fluid 1
2	fluid 2

References

[1] G.A. Baker, T.A. Oliphant, An implicit numerical method for solving the two-dimensional heat equation, Quart. Appl. Math. 17 (4) (1960) 361–373.

[2] S. Bergero, S. Chiari, Experimental analysis of air humidification/dehumidification processes using hydrophobic capillary contactors, Appl. Therm. Eng. 21 (2001) 1119–1135.

[3] V.Y. Dindore, A.H.G. Cents, D.W.F. Brilman, G.F. Versteeg, Shell-side dispersion coefficients in a rectangular cross-flow hollow fiber membrane module, Chem. Eng. Res. Des. (2005) in press.

[4] A. Gabelman, S. Hwang, Hollow fiber membrane contactors, J. Membr. Sci. 159 (1999) 61–106.

[5] P.H.M. Feron, A.E. Jansen, CO_2 separation with polyolefin membrane contactors and dedicated absorption liquids: performance and prospects, Sep. Purif. Technol. 27 (2002) 231–242.

[6] K.A. Hoff, Modeling and experimental study of carbon dioxide absorption in a membrane contactor, Ph.D. Thesis, Norwegian University of Science and Technology, Norway, 2003.

[7] A.E. Jansen, R. Klaassen, P.H.M. Feron, J.H. Hanemaaijer, B.Ph. ter Meulen, Membrane gas absorption processes in environmental applications, in: J.G. Crespo, K.W. Boddeker (Eds.), Membrane Processes in Separation and Purification, Kluwer Academic Publishers, Dordrecht, 1994, pp. 343–356.

[8] H. Kreulen, C.A. Smolders, G.F. Versteeg, W.P.M. van Swaaij, Microporous hollow-fiber membrane modules as gas–liquid contactors. 1. Physical mass transfer processes—a specific application—mass transfer in highly viscous liquids, J. Membr. Sci. 78 (3) (1993) 197–216.

[9] W. Nusselt, Der warmeubergang im kreuzstorm, Zeitschrift des Vereines deutscher Ingenieur 55 (1911) 2021–2024.

[10] D.M. Smith, Mean temperature difference in cross-flow, Engineering 138 (1934) 479–482, 606–607.

[11] G.F. Versteeg, J.A.M. Kuipers, F.P.M. van Beckum, W.P.M. van Swaaij, Mass transfer with complex chemical reactions. I. Single reversible reaction, Chem. Eng. Sci. 44 (8) (1989) 1715–1721.

[12] G.F. Versteeg, W.P.M. van Swaaij, Solubility and diffusivity of acid gases in aqueous alkanolamine solutions, J. Chem. Eng. Data 33 (1988) 29–34.

[13] K.L. Wang, E.L. Cussler, Baffled membrane modules made with hollow fiber fabric, J. Membr. Sci. 85 (1993) 265–278.

[14] S.R. Wickramasinghe, M.J. Semmens, E.L. Cussler, Mass transfer in various hollow fiber geometries, J. Membr. Sci. 69 (1992) 235–250.